IEEE Photonics Journal
An IEEE Photonics Society Publication

Open Access

Discussion of the Epsilon-Near-Zero Effect of Graphene in a Horizontal Slot Waveguide

Volume 6, Number 3, June 2014

Min-Suk Kwon

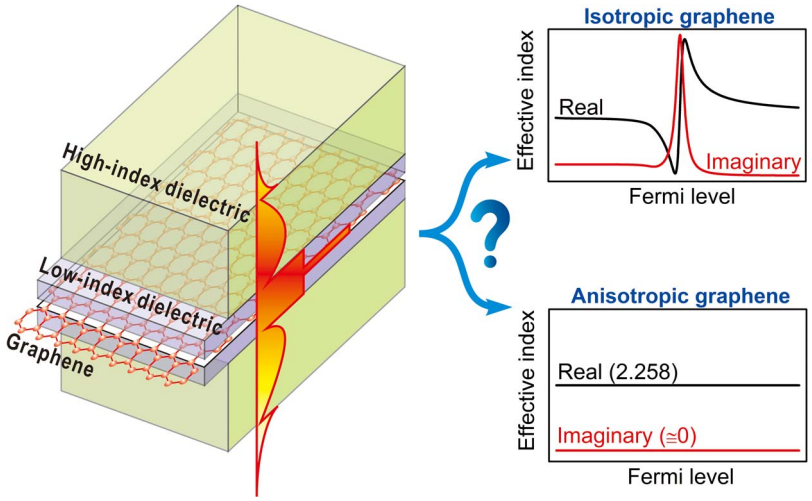

DOI: 10.1109/JPHOT.2014.2326667
1943-0655 © 2014 IEEE

Discussion of the Epsilon-Near-Zero Effect of Graphene in a Horizontal Slot Waveguide

Min-Suk Kwon

School of Electrical and Computer Engineering, Ulsan National Institute of Science and Technology (UNIST), Ulsan 689-798, Korea

DOI: 10.1109/JPHOT.2014.2326667

Manuscript received April 24, 2014; revised May 15, 2014; accepted May 16, 2014. Date of publication May 23, 2014; date of current version June 5, 2014. This work was supported by the Basic Science Research Program through the National Research Foundation of Korea (NRF) funded by the Ministry of Education under Grant 2013R1A1A2A10062227. Corresponding author: M.-S. Kwon (e-mail: mskwon@unist.ac.kr).

Abstract: Horizontal slot waveguides based on graphene have been considered an attractive structure for optical waveguide modulators for transverse magnetic (TM) modes. Graphene is embedded in the slot region of a horizontal slot waveguide. If graphene were treated as an isotropic material and its dielectric constant were made close to zero by adjusting its Fermi level, the surface-normal electric field component of the fundamental TM mode of a horizontal slot waveguide might be highly enhanced in graphene. This could cause a large increase in the attenuation coefficient of the mode. This is called the epsilon-near-zero (ENZ) effect. This paper discusses that graphene needs to be treated as an anisotropic material that has an almost real surface-normal dielectric constant component. Then, the ENZ effect does not exist. Approximate analytic expressions and numerical simulation are used for the discussion, and they demonstrate that horizontal slot waveguides are not appropriate for graphene-based modulators for TM modes.

Index Terms: Waveguide devices, optical properties of photonic materials, graphene.

1. Introduction

Graphene, a monolayer of carbon atoms arranged in a honeycomb lattice, has been a very promising material for diverse electronic and photonic devices because of its exceptional properties like the highest intrinsic mobility [1]. A few examples of photonic devices based on graphene are photodetectors [2], [3], polarizers [4], and tunable optical antennas [5], [6]. In particular, graphene is considered as an active material suitable for optical waveguide modulators since it interacts strongly with light and its optical conductivity is electrically controllable. Thus graphene-based modulators are expected to have a small footprint, consume small energy, and operate at a high speed over a broad spectral range.

Since a normal silicon waveguide with one or two graphene layers on its top was experimentally demonstrated as an electro-absorption modulator [7], [8], a variety of graphene-based modulators have been theoretically studied [9]–[13]. The recent studies have focused on the development of a waveguide which supports a waveguide mode with the maximum electric field in a graphene layer. In such a waveguide, the electrically-tunable optical conductivity of graphene can effectively affect the effective index of the waveguide mode. Consequently, it is possible to reduce modulator dimensions. Horizontal slot waveguides have been considered as such a waveguide [10]–[13]. Horizontal slot waveguides without graphene have been actively studied already [14], [15]. A

horizontal slot waveguide with graphene has a slot region which is a stack of thin low-index dielectric layers and graphene layers, and the stack is sandwiched by two high-index dielectric layers, two metal layers, or a high-index dielectric layer and a metal layer. The vertical electric field component of the fundamental transverse-magnetic (TM) mode of the horizontal slot waveguide is strongly enhanced in the slot region due to the discontinuity of the vertical electric field component at a layer-layer interface or excitation of a surface plasmon polariton at a metal-dielectric interface. This enhancement could become dramatically large in the graphene layers in the slot region such that the attenuation of the fundamental TM mode could increase rapidly if the Fermi level E_F of graphene is appropriately adjusted. This is called the epsilon-near-zero (ENZ) effect. Based on the ENZ effect, electroabsorption modulators with a length smaller than 1 μm were proposed [10]–[12], and a Mach-Zehnder modulator with a high extinction ratio was proposed [13].

Although the modulators based on the ENZ effect seem very promising, there is a question about the existence of the ENZ effect. The question stems from the following inference. Since graphene is one atom thick and its π electrons cause electric conduction in its plane, it has been treated as a boundary with in-plane conductivity $\sigma_{\parallel}$ when the electromagnetic or optical characteristics of a structure with graphene are analyzed [4], [16] (this treatment is hereafter called the conducting boundary model). However, to analyze a complex structure with graphene, graphene has been also treated as a thin dielectric layer with a finite thickness d_g [17]. When graphene is normal to the z axis, its effective dielectric constant is a diagonal tensor with in-plane components ε_{xx} and ε_{yy} and a surface-normal component ε_{zz}. $\varepsilon_{xx} = \varepsilon_{yy}$, and $\varepsilon_{yy} = \varepsilon_{\parallel\infty} + i\sigma_{\parallel}/(\omega\varepsilon_0 d_g)$. The relation of ε_{zz} and surface-normal conductivity $\sigma_{\perp}$ is given by $\varepsilon_{zz} = \varepsilon_{\perp\infty} + i\sigma_{\perp}/(\omega\varepsilon_0 d_g)$. $\varepsilon_{\parallel\infty}$ and $\varepsilon_{\perp\infty}$ are background dielectric constants. In many cases, it has been assumed that $\varepsilon_{\perp\infty} = \varepsilon_{\parallel\infty}$ and $\sigma_{\perp} = \sigma_{\parallel}$. In other words, graphene is treated as an isotropic material (this treatment is hereafter called the isotropic graphene model). The dominant electric field component of the fundamental TM mode is affected by ε_{zz}, and $|\varepsilon_{zz}|$ can be made as small as possible if E_F becomes equal to a specific value. For example, at the telecom wavelength of 1.55 μm, $|\varepsilon_{zz}| = 0.327$ for $E_F = 0.515$ eV in [10], and $|\varepsilon_{zz}| = 0.707$ for $E_F = 0.51$ eV in [12]. Hence, the ENZ effect could exist. However, in the case of graphite, $|\sigma_{\perp}|$ is smaller than $|\sigma_{\parallel}|$ by a factor of $\sim$0.01 [18]. Since graphene is considered as a single layer of graphite and the π electrons of graphene move in its plane, $|\sigma_{\perp}|$ of graphene is reasoned to be much smaller than $|\sigma_{\parallel}|$ of graphene. Therefore, $|\varepsilon_{zz}|$ may not be made close to zero. The existence of the ENZ effect is questioned from this aspect. Naturally, the question requires us to treat graphene as an anisotropic material (this treatment is hereafter called the anisotropic graphene model) when we analyze horizontal slot waveguides. Actually, spectroscopic ellipsometry measurement elucidated that graphene can be modeled as a uniaxial material [19]. By using a one-dimensional slot waveguide with a graphene layer, this paper shows why the ENZ effect exists in the case of the isotropic graphene model. This paper also demonstrates that the anisotropic graphene model and the conducting boundary model yield similar analysis results. These results confirm that the ENZ effect does not exist in the case of the anisotropic graphene model. Finally, this paper discusses that horizontal slot waveguides are not appropriate for graphene-based modulators for TM modes.

2. One-Dimensional Symmetric Slot Waveguide With Graphene

The one-dimensional slot waveguide consists of layers which are normal to the z-axis. It is symmetric about the xy-plane as shown in Fig. 1. Graphene is treated as an isotropic or anisotropic dielectric layer of thickness $2d_1 = d_g$, and the layer is centered at $z = 0$. The graphene layer is sandwiched by the same low-index dielectric layers of thickness d_2 and refractive index n_2. This stack is the slot region sandwiched by the same high-index dielectric layers of thickness d_3 and refractive index n_3. The material above and below the high-index layers has a refractive index n_4. n_2, n_3, and n_4 are real. For strong enhancement of the surface-normal electric field component of the fundamental TM mode in the slot region, d_2 is determined such that $d_2 \ll \lambda/n_2$, where λ is the free-space wavelength. In addition, d_3 is appropriately chosen for the strong enhancement. The

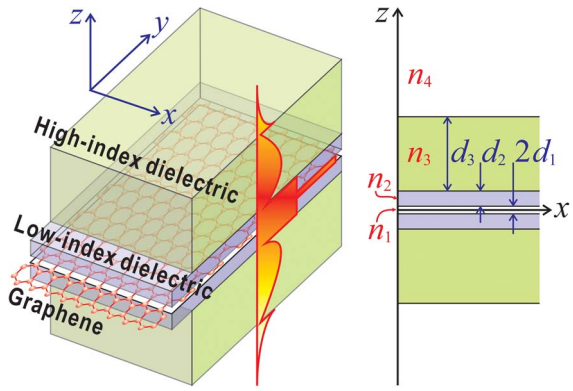

Fig. 1. Geometrical structure of the studied horizontal slot waveguide. It is uniform in the *x*-direction, and symmetric about the *xy*-plane. The fundamental TM mode of the waveguide, which has the schematically depicted distribution of the *z* component of the electric field, propagates in the *y*-direction. Graphene is treated as the dielectric layer of refractive index n_1 and thickness $2d_1$ in the cases of the isotropic and anisotropic graphene models.

magnetic field of the mode is expressed by $\mathbf{H} = \hat{x} H_x(z) \exp[i(\beta y - \omega t)]$, where β is the propagation constant of the mode. From Maxwell's equations and the symmetry of the mode

$$H_x(z) = H_0 \begin{cases} \cosh(\phi)\cosh(\gamma_1 z)/\cosh(\gamma_1 d_1), & |z| < d_1, \\ \cosh[\gamma_2(|z| - d_1) + \phi], & d_1 < |z| < d_1 + d_2, \\ \cosh(\gamma_2 d_2 + \phi)\cos[\kappa_3(|z| - d_1 - d_2) + \psi]/\cos(\psi), & d_1 + d_2 < |z| < d_1 + d_2 + d_3, \\ \cosh(\gamma_2 d_2 + \phi)\cos(\kappa_3 d_3 + \psi) & \\ \quad \times \exp[-\gamma_4(|z| - d_1 - d_2 - d_3)]/\cos(\psi), & |z| > d_1 + d_2 + d_3. \end{cases} \quad (1)$$

In this expression, $\gamma_1 = \sqrt{(\beta^2/\varepsilon_{zz} - k^2)\varepsilon_{yy}}$, $k = 2\pi/\lambda$, $\gamma_j = \sqrt{\beta^2 - k^2 n_j^2}$ for $j = 2$ or 4, and $\kappa_3 = \sqrt{k^2 n_3^2 - \beta^2}$. The constants ϕ and ψ and β are determined by solving the equations

$$\tanh(\phi) = \frac{\gamma_1}{\varepsilon_{yy}} \frac{n_2^2}{\gamma_2} \tanh(\gamma_1 d_1), \quad \tan(\psi) = -\frac{\gamma_2}{n_2^2} \frac{n_3^2}{\kappa_3} \tanh(\gamma_2 d_2 + \phi), \quad \tan(\kappa_3 d_3 + \psi) = \frac{n_3^2}{\kappa_3} \frac{\gamma_4}{n_4^2}, \quad (2)$$

which are derived from the continuity of the *y* component of the electric field at the interfaces in Fig. 1. H_0 is a normalization constant such that $(1/2)\int_{-\infty}^{\infty} \mathrm{Re}\{\beta |H_x|^2/[\omega \varepsilon_0 \varepsilon_z(z)]\} dz = 1$ W/m, where $\varepsilon_z(z)$ is equal to ε_{zz} in layer 1 and n_j^2 in layer *j*, $j = 2, 3, 4$.

Since $d_g = 0.335$ nm [19], $d_1/\lambda \ll 1$ for $\lambda = 1.55$ μm. Moreover, as shown below, even the minimum value of $|\varepsilon_{yy}|$ is much larger than d_1/λ. Then, the first equation of (2) approximately becomes

$$\phi \approx (N_{\mathrm{eff}}^2/\varepsilon_{zz} - 1) n_2^2 k^2 d_1/\gamma_2 \approx 0, \quad (3)$$

where $N_{\mathrm{eff}} \equiv \beta/k$ is the effective index of the mode. When $\phi \approx 0$, ψ is also approximately equal to zero since $d_2 \ll \lambda/n_2$. Then, the ratio η_z between the magnitudes of the *z* component of the electric field, E_z, at $z = (d_1)^-$ and $z = (d_1 + d_2 + d_3)^+$ is approximately

$$\eta_z \approx \left| 1 + \left(\frac{n_3^2}{\kappa_3} \frac{\gamma_4}{n_4^2} \right)^2 \right|^{1/2} \frac{n_4^2}{|\varepsilon_{zz}|}. \quad (4)$$

In addition, the ratio η_y between the magnitudes of the *y* component of the electric field, E_y, at $z = (d_1)^-$ and $z = (d_1 + d_2 + d_3)^+$ is approximately

$$\eta_y \approx \left| 1 + \left(\frac{n_3^2}{\kappa_3} \frac{\gamma_4}{n_4^2} \right)^2 \right|^{1/2} \left| \frac{n_4^2}{\gamma_4} \left(\frac{N_{\mathrm{eff}}^2}{\varepsilon_{zz}} - 1 \right) k^2 d_1 \right|. \quad (5)$$

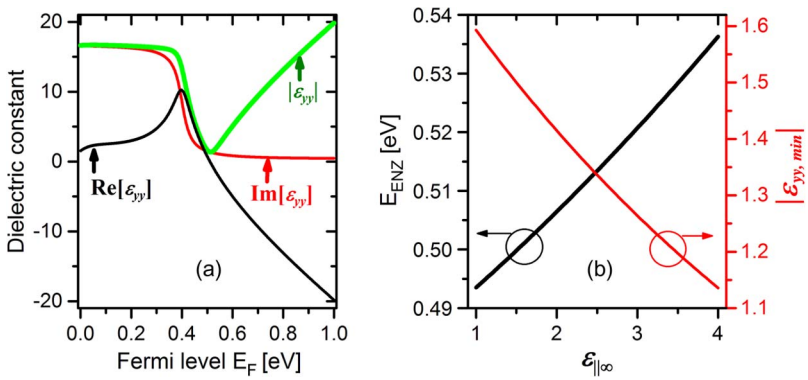

Fig. 2. Dielectric constant of graphene. (a) Real and imaginary parts and magnitude of the in-plane dielectric constant component ε_{yy} of graphene vs. Fermi level E_F of graphene. ε_{yy} is given by $\varepsilon_{\|\infty} + i\sigma_{\|}/(\omega\varepsilon_0 d_g)$. $\varepsilon_{\|\infty} = 2.5$ in (a). (b) Relation between the Fermi level E_{ENZ} at which ε_{yy} has the minimum magnitude $|\varepsilon_{yy,\min}|$ and $\varepsilon_{\|\infty}$ (black curve). The red curve represents the relation of $|\varepsilon_{yy,\min}|$ to $\varepsilon_{\|\infty}$.

Compared to η_z, η_y is very small and close to zero. Therefore, the z component of the electric field is highly dominant in layer 1, i.e., the graphene layer. This fact and the assumption that n_2, n_3, and n_4 are real result in the expression of the attenuation coefficient α of the mode [20], which is

$$\alpha = \frac{1}{2}\omega\varepsilon_0 \int_{-\infty}^{\infty} \left\{ \mathrm{Im}[\varepsilon_z(z)]|E_z|^2 + \mathrm{Im}[\varepsilon_y(z)]|E_y|^2 \right\} dz \simeq \int_0^{d_1} \mathrm{Im}[\varepsilon_{zz}] \frac{|\beta|^2}{\omega\varepsilon_0} \left| \frac{H_x}{\varepsilon_{zz}} \right|^2 dz \approx |H_0|^2 \frac{|\beta|^2 d_1}{\omega\varepsilon_0} \frac{\mathrm{Im}[\varepsilon_{zz}]}{|\varepsilon_{zz}|^2}, \quad (6)$$

where $\varepsilon_y(z)$ is equal to ε_{yy} in layer 1 and n_j^2 in layer j, $j = 2, 3, 4$. The electric field components of the mode satisfy $E_y = i(dH_x/dz)/[\omega\varepsilon_0\varepsilon_y(z)]$ and $E_z = (\beta H_x)/[\omega\varepsilon_0\varepsilon_z(z)]$.

For the in-plane conductivity of graphene, an analytic expression derived within the random-phase approximation [21] is used, which is

$$\sigma_{\|} = \frac{i8\sigma_0}{\pi} \frac{E_{th}}{E_{ph} + iE_s} \ln\left[2\cosh\left(\frac{E_F}{2E_{th}}\right)\right] + \sigma_0 \left[\frac{1}{2} + \frac{1}{\pi}\tan^{-1}\left(\frac{E_{ph} - 2E_F}{2E_{th}}\right) - \frac{i}{2\pi}\ln\frac{(E_{ph} + 2E_F)^2}{(E_{ph} - 2E_F)^2 + 4E_{th}^2}\right], \quad (7)$$

where $\sigma_0 \equiv e^2/(4\hbar)$ is the universal conductivity of graphene (e is the charge of an electron and $\hbar$ is the reduced Planck constant), $E_{th} = k_B T$ is thermal energy in eV (k_B is the Boltzmann constant, and T is the temperature), $E_{ph} = hc/\lambda$ is photon energy in eV (h is the Planck constant), and $E_s = \hbar/\tau$ is scattering energy in eV for the scattering time τ. Fig. 2(a) shows ε_{yy} vs. E_F for $\lambda = 1.55$ μm, $T = 300$ K, $\tau = 0.1$ ps, and $\varepsilon_{\|\infty} = 2.5$ (these values are used for the following simulation). Since interband transitions do not happen if $E_F > E_{ph}/2 = 0.4$ eV, $\mathrm{Im}[\varepsilon_{yy}]$ rapidly approaches zero. $\mathrm{Re}[\varepsilon_{yy}]$ decreases monotonically for $E_F > 0.4$ eV since intraband transitions dominate. $|\varepsilon_{yy}|$ has its minimum $|\varepsilon_{yy,\min}|$ at $E_F = E_{ENZ}$. Fig. 2(b) shows $|\varepsilon_{yy,\min}|$ and E_{ENZ} as functions of $\varepsilon_{\|\infty}$. For $\varepsilon_{\|\infty} = 2.5$, $E_{ENZ} = 0.513$ eV, and $\varepsilon_{yy,\min} = -0.202 + i1.32$. As mentioned above, $|\varepsilon_{yy,\min}|$ is much larger than d_1/λ. However, $\varepsilon_{yy,\min}$ is not so close to zero. Actually, E_{ENZ} and $\varepsilon_{yy,\min}$ depend on which analytic expression of σ_g is used. For example, if the analytic expression in [22] is employed, $E_{ENZ} = 0.514$ eV, and $\varepsilon_{yy,\min} = -0.026 + i0.212$. However, this is not critical in the following discussion of the ENZ effect.

In the case of the anisotropic graphene model, $\sigma_{\perp}$ is made equal to zero as assumed in [23], [24]. $\varepsilon_{\perp\infty}$ was set to 1 [23] or 2.5 which comes from the dielectric constant of graphite [24]. In this paper, $\varepsilon_{\perp\infty} = \varepsilon_{\|\infty} = 2.5$. Now, by using (3), (4), and (6), it is possible to discuss the ENZ effect depending on how graphene is modeled. First, if the isotropic graphene model is used, ϕ is a very small complex number since ε_{zz} is complex. Then, N_{eff} should be complex to satisfy the remaining equations of (2). However, ϕ is a very small real number for the anisotropic graphene model since

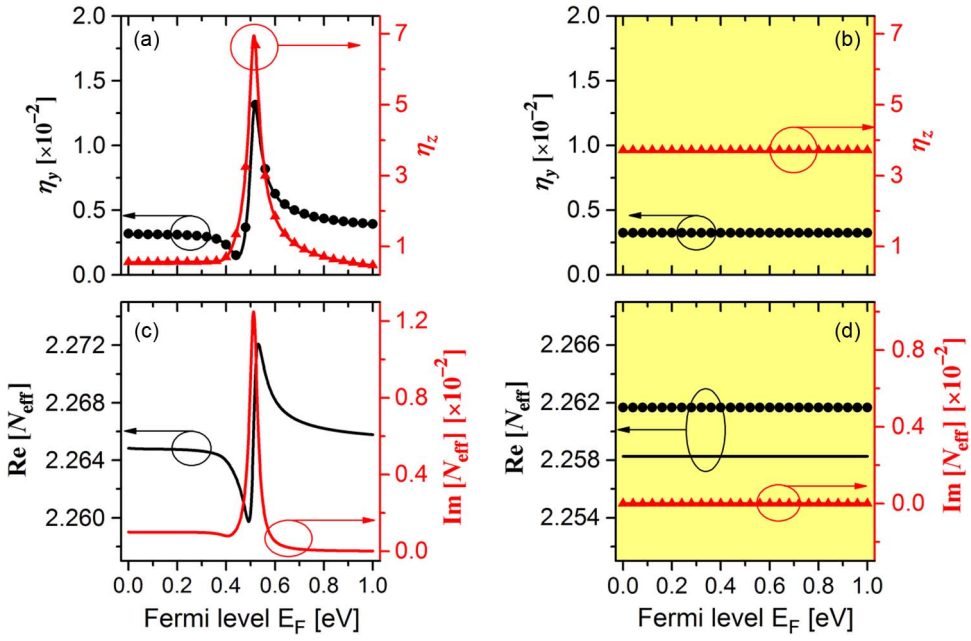

Fig. 3. Electric field enhancement factors η_z and η_y and effective index N_{eff} of the fundamental TM mode of the slot waveguide in Fig. 1. (a) and (b) show the relations of η_z and η_y to E_F in the cases of the isotropic graphene model and the anisotropic graphene model, respectively. The solid lines are obtained by solving (2) and using (1). The symbols are obtained by using (4) and (5). (c) and (d) show the relations of N_{eff} to E_F in the cases of the isotropic graphene model and the anisotropic graphene model, respectively. The solid lines are obtained by solving (2). The symbols in (d) are obtained by using the transfer matrix method based on the conducting boundary model.

ε_{zz} is real. Hence, N_{eff} can be almost real. This indicates that the ENZ effect that the mode attenuation rapidly increases does not exist in the case of the anisotropic graphene model. Second, η_z becomes very large, i.e., strong enhancement of the surface-normal electric field component can be achieved in the case of the isotropic graphene model with $E_F = E_{ENZ}$. However, η_z is just a finite number almost independent of E_F in the case of the anisotropic graphene model. Finally, α is nonzero, and it becomes large in the case of the isotropic graphene model with $E_F = E_{ENZ}$. In contrast, α is almost equal to zero in the case of the anisotropic graphene model. All these things demonstrate that the ENZ effect exists just in the case of the isotropic graphene model. However, it does not exist in the case of the anisotropic graphene model which is more realistic. This is confirmed by the following result of simulation.

For the simulation of the slot waveguide, n_2, n_3, and n_4 are set to the refractive indices of aluminum oxide (Al_2O_3), silicon, and air, respectively, i.e., $n_2 = 1.746$, $n_3 = 3.455$, and $n_4 = 1$. In addition, d_2 and d_3 are set to 10 nm and 150 nm, respectively. By using the function fsolve in Optimization Toolbox of MATLAB, (2) is solved to find β. The calculated values of η_z and η_y are shown as functions of E_F in Fig. 3(a) and (b) for the isotropic and anisotropic graphene models, respectively. The values obtained from (4) and (5) are in good agreement with the values obtained by solving (2) and using (1). In the case of the isotropic graphene model, η_z rapidly increases and decreases near E_{ENZ}, and η_y is much smaller than η_z. For E_F near E_{ENZ}, the surface-normal electric field component is highly enhanced in the graphene layer. It experiences the imaginary part of $\varepsilon_{zz} = \varepsilon_{yy}$ such that the attenuation coefficient of the mode becomes large. Therefore, Im$[N_{eff}]$ changes similarly to η_z with respect to E_F as shown in Fig. 3(c). Re$[N_{eff}]$ changes significantly and almost antisymmetrically near E_{ENZ}. This is the ENZ effect which has been discussed and utilized in [10]–[13]. However, in the case of the anisotropic graphene model, η_z and η_y are constant since ε_{zz} is independent of E_F. In addition, N_{eff} is an almost real constant as discussed above. Therefore, the ENZ effect does not exist. The relation between N_{eff} and E_F is similar to that obtained by using the conducting boundary model. When the conducting boundary model is used, the characteristic

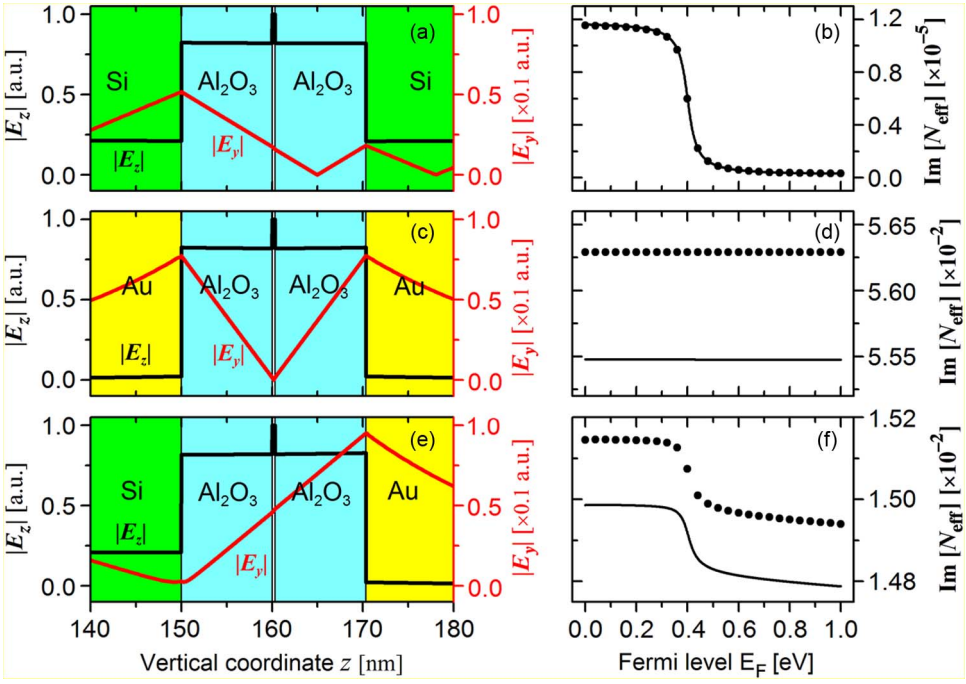

Fig. 4. Mode characteristics of the fundamental TM modes of the three kinds of one-dimensional slot waveguides. $|E_y|$ (in-plane component) is compared with $|E_z|$ (surface-normal component) in (a), (c), and (e). (b), (d), and (f) show how the imaginary part of the effective index, $\mathrm{Im}[N_{\mathrm{eff}}]$, changes with respect to E_F for the three slot waveguides. The solid lines and the symbols are obtained by using the anisotropic graphene model and the conducting boundary model, respectively.

equation or dispersion equation of N_{eff} is derived by using the transfer matrix method (TMM) [25] satisfying the boundary condition $H_x(z_g^+) - H_x(z_g^-) = \sigma_{\parallel} E_y(z_g^+) = \sigma_{\parallel} E_y(z_g^-)$ at the position of the graphene layer, z_g. Then, the characteristic equation is solved to find N_{eff} by using the function fsolve. There is a small difference between the real parts of N_{eff} calculated by using the conducting boundary model and the anisotropic graphene model. The difference decreases as $\varepsilon_{\perp\infty}$ and $\varepsilon_{\parallel\infty}$ increase. When the conducting boundary model is used, the fact that $\mathrm{Im}[N_{\mathrm{eff}}] = 0$ is deduced from the symmetry of the structure in Fig. 1. Because of the symmetry, H_x is an even function of z, and dH_x/dz (i.e., E_y) is an odd function of z. Therefore, the graphene has no influence on N_{eff} since $E_y = 0$ at the graphene boundary, and N_{eff} is real.

3. Discussion of Horizontal Slot Waveguides for Graphene-Based Modulators

It has just been shown that the ENZ effect does not exist in the symmetric slot waveguide in Fig. 1 when the symmetric slot waveguide is analyzed by using the anisotropic graphene model or the conducting boundary model. Since its effective index is independent of E_F, it cannot be used for a graphene-based modulator. Now, it is necessary to check whether other horizontal slot waveguides are appropriate for graphene-based modulators. Three kinds of one-dimensional slot waveguides are analyzed here. They have an Al_2O_3-graphene-Al_2O_3 stack sandwiched by two Si layers [Fig. 4(a) and (b)], two gold layers [Fig. 4(c) and (d)], or a Si layer and a gold layer [Fig. 4(e) and (f)], all of which are 150 nm thick. Their substrate and cover are silicon dioxide (SiO_2) and air, respectively. The three horizontal slot waveguides are analyzed by using the TMM based on the anisotropic graphene model or the conducting boundary model. The distribution of the electric field of the fundamental TM mode of each slot waveguide around the stack is shown in Fig. 4(a), (c), and (e). For comparison, the magnitudes of the in-plane and surface-normal electric field components E_y and E_z are normalized to the peak value of $|E_z|$ in the stack. $|E_y|$ is more than one order of

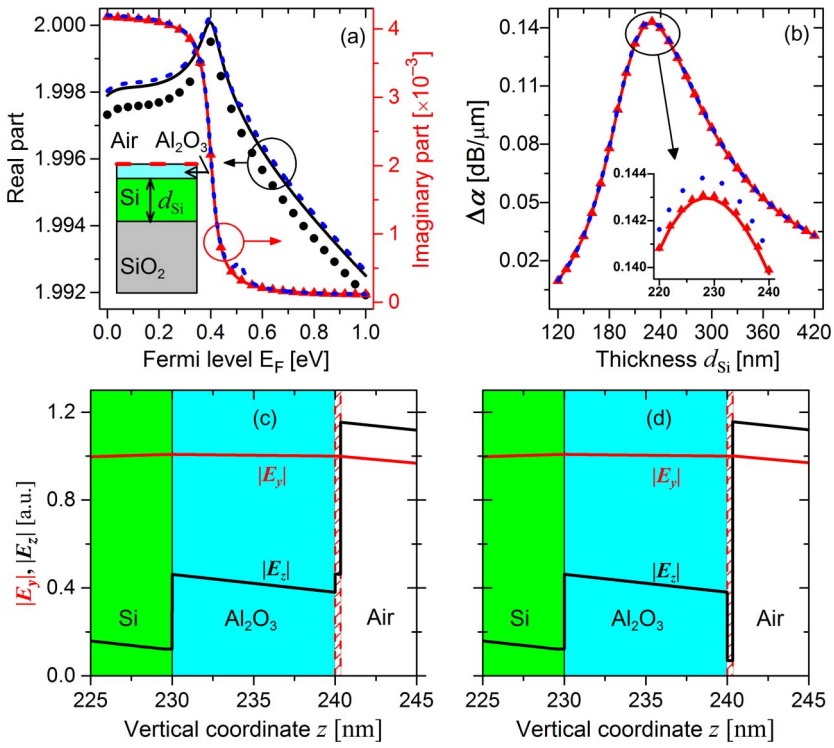

Fig. 5. Mode characteristics of the fundamental TM mode of the slab waveguide with graphene on its top as shown in the inset of (a). (a) Relations of the real and imaginary parts of the effective index to E_F. (b) Relation of $\Delta\alpha$ to d_{Si}. $\Delta\alpha$ is calculated by subtracting the attenuation coefficient for $E_F = 1$ eV from that for $E_F = 0$ eV. The black and red solid lines in (a) and (b) are obtained by using the TMM based on the anisotropic graphene model. The black and red symbols in (a) and (b) are obtained by using the TMM based on the conducting boundary model. The dashed blue lines in (a) and (b) are obtained by using the TMM based on the isotropic graphene model. (c) Distributions of $|E_y|$ (in-plane component) and $|E_z|$ (surface-normal component) in the case of the anisotropic graphene model for $E_F = 0$ eV. (d) Distributions of $|E_y|$ and $|E_z|$ in the case of the isotropic graphene model for $E_F = 0$ eV.

magnitude smaller than $|E_z|$ in the graphene layer embedded in each slot region. This can be approximately explained as follows. E_y just outside the slot region is proportional to $|(N_{eff}^2 - n^2)^{1/2}/n^2|$, where n is the refractive index of the layer on or beneath each slot region and N_{eff} is the effective index of the fundamental TM mode of each horizontal slot waveguide. This number is small since $|n|$ is large for a high-index dielectric layer or a metal layer. Therefore, E_y is small in each slot region due to its continuity at the boundaries of each slot region. Since E_y is very small in the graphene layer, the in-plane dielectric constant component or conductivity of graphene does not significantly affect N_{eff}. This can be confirmed from Fig. 4(b), (d), and (f). The decrease of $\mathrm{Im}[N_{eff}]$ caused by the increase of E_F is smaller than 2×10^{-4}. This means that the attenuation coefficient decrease of each slot waveguide is smaller than 7×10^{-3} dB/μm. As shown in Fig. 3, the values of $\mathrm{Im}[N_{eff}]$ calculated by using the anisotropic graphene model are close to those calculated by using the conducting boundary model. Consequently, the characteristics of each slot waveguide are not efficiently tuned by adjusting E_F. Therefore, all the horizontal slot waveguides are not suitable for optical waveguide modulators for TM modes.

Actually, a slab waveguide with a graphene layer on its top is better for optical waveguide modulators for TM modes than the horizontal slot waveguides. This is confirmed by simulation of a slab waveguide consisting of graphene, Al_2O_3, and silicon. Its cover and substrate are air and SiO_2, respectively. The thickness of the Al_2O_3 layer is 10 nm, and the thickness of the Si layer, d_{Si} is a variable. The effective index of the fundamental TM mode is calculated by using the TMM. It is shown with respect to E_F in Fig. 5(a) for $d_{Si} = 230$ nm. Its real and imaginary parts change similarly to the real and imaginary parts of ε_{yy}, respectively. Interestingly, the values of the effective index

calculated by using the isotropic graphene model are similar to those calculated by using the anisotropic graphene model or the conducting boundary model. This can be deduced from the profiles of the in-plane and surface-normal electric field components E_y and E_z of the fundamental mode, which are shown in Fig. 5(c) and (d) in the cases of the anisotropic and isotropic graphene models, respectively. For comparison, $|E_y|$ and $|E_z|$ are normalized to the peak value of $|E_y|$ in the graphene layer. When the isotropic graphene model is used, $|E_z|$ is much smaller than $|E_y|$ in the graphene layer such that the in-plane dielectric constant component of graphene dominantly affects the effective index as in the case of the anisotropic graphene model. Hence, the effective index changes little depending on which graphene model is used. The slab waveguide is an example that shows the reason why the isotropic graphene model has been used for reasonable analysis in many cases. The difference between the attenuation coefficients for $E_F = 0$ eV and $E_F = 1$ eV, $\Delta\alpha$(in dB/μm) is shown with respect to d_{Si} in Fig. 5(b). The difference is maximum at $d_{Si} = 230$ nm, which is 0.143 dB/μm and similar to the experimentally observed value in [7]. If d_{Si} is small, the magnetic field H_x of the mode is not strongly confined in the Si layer, and it slowly changes in the graphene layer. Hence, E_y proportional to dH_x/dz is small. If d_{Si} is large, H_x is strongly confined in the Si layer, and it is small in the graphene layer. Hence, E_y is also small. Therefore, there is an optimal value of d_{Si} at which $\Delta\alpha$ is maximized.

4. Conclusion

In summary, the ENZ effect might exist in a horizontal slot waveguide only if graphene were an isotropic material. In other words, if the surface-normal dielectric constant component of graphene were made close to zero, the surface-normal electric field component would be highly enhanced in the graphene layer in the slot region of the waveguide. Consequently, the fundamental TM mode of the waveguide could have a large attenuation coefficient. However, graphene needs to be treated as a conducting boundary or an anisotropic material with an almost real surface-normal dielectric constant component. Then, the ENZ effect does not exist in a horizontal slot waveguide. These things have been confirmed by using the analytic expressions and the numerical calculations. They have led to the conclusion that horizontal slot waveguides may not be efficient in modulating TM modes. To complete this discussion, in the future, it is necessary to experimentally determine the surface-normal dielectric constant component of graphene and confirm that it is really almost real.

References

[1] P. Avouris, "Graphene: Electronic and photonic properties and devices," *Nano Lett.*, vol. 10, no. 11, pp. 4285–4294, Nov. 2010.
[2] X. Gan *et al.,* "Chip-integrated ultrafast graphene photodetector with high responsivity," *Nat. Photon.*, vol. 7, no. 11, pp. 883–887, Nov. 2013.
[3] A. Pospischil *et al.,* "CMOS-compatible graphene photodetector covering all optical communication bands," *Nat. Photon.*, vol. 7, no. 11, pp. 892–896, Nov. 2013.
[4] Q. Bao *et al.,* "Broadband graphene polarizer," *Nat. Photon.*, vol. 5, no. 7, pp. 411–415, Jul. 2011.
[5] J. Kim *et al.,* "Electrical control of optical plasmon resonance with graphene," *Nano Lett.*, vol. 12, no. 11, pp. 5598–5602, Nov. 2012.
[6] Y. Yao *et al.,* "Broad electrical tuning of graphene-loaded plasmonic antennas," *Nano Lett.*, vol. 13, no. 3, pp. 1257–1264, Mar. 2013.
[7] M. Liu *et al.,* "A graphene-based broadband optical modulator," *Nature*, vol. 474, no. 7349, pp. 64–67, Jun. 2011.
[8] M. Liu, X. Yin, and X. Zhang, "Double-layer graphene optical modulator," *Nano Lett.*, vol. 12, no. 3, pp. 1482–1485, Mar. 2012.
[9] S. J. Koester, H. Li, and M. Li, "Switching energy limits of waveguide-coupled graphene-on-graphene optical modulators," *Opt. Exp.*, vol. 20, no. 18, pp. 20 330–20 341, Aug. 2012.
[10] Z. Lu and W. Zhao, "Nanoscale electro-optic modulators based on graphene-slot waveguides," *J. Opt. Soc. Amer. B, Opt. Phys.*, vol. 29, no. 6, pp. 1490–1496, Jun. 2012.
[11] J. Gosciniak and D. T. H. Tan, "Graphene-based waveguide integrated dielectric-loaded plasmonic electro-absorption modulators," *Nanotechnology*, vol. 24, no. 18, pp. 185202-1–185202-9, May 2013.
[12] J. Gosciniak and D. T. H. Tan, "Theoretical investigation of graphene-based photonic modulators," *Sci. Rep.*, vol. 3, pp. 01897-1–01897-6, May 2013.
[13] L. Yang *et al.,* "Low-chirp high-extinction-ratio modulator based on graphene-silicon waveguide," *Opt. Lett.*, vol. 38, no. 14, pp. 2512–2515, Jul. 2013.

[14] R. Sun *et al.,* "Horizontal single and multiple slot waveguides: Optical transmission at $\lambda = 1550$ nm," *Opt. Exp.*, vol. 15, no. 26, pp. 17967–17972, Dec. 2007.
[15] C. Xiong *et al.,* "Active silicon integrated nanophotonics: Ferroelectric$BaTiO_3$ devices," *Nano Lett.*, vol. 14, no. 3, pp. 1419–1425, Mar. 2014.
[16] C. Xu, Y. Jin, L. Yang, J. Yang, and X. Jiang, "Characteristics of electro-refractive modulating based on graphene-oxide-silicon waveguide," *Opt. Exp.*, vol. 20, no. 20, pp. 22 398–22 405, Sep. 2012.
[17] A. Vakil and N. Engheta, "Transformation optics using graphene," *Science*, vol. 332, no. 6035, pp. 1291–1294, Jun. 2011.
[18] L. A. Falkovsky, "Anisotropy of graphite optical conductivity," *JETP Lett.*, vol. 92, no. 5, pp. 348–351, Sep. 2010.
[19] V. G. Kravets *et al.,* "Spectroscopic ellipsometry of graphene and an exciton-shifted van Hove peak in absorption," *Phys. Rev. B, Condens. Matter*, vol. 81, no. 15, pp. 155413-1–155413-6, Apr. 2010.
[20] A. W. Snyder and J. D. Love, *Optical Waveguide Theory*. London, U.K.: Chapman & Hall, 1983.
[21] L. A. Falkovsky, "Optical properties of graphene and IV-VI semiconductors," *Phys.-Usp.*, vol. 51, no. 9, pp. 887–897, Sep. 2008.
[22] E. Simsek, "A closed-form approximate expression for the optical conductivity of graphene," *Opt. Lett.*, vol. 38, no. 9, pp. 1437–1439, May 2013.
[23] S. H. Mousavi *et al.,* "Inductive tuning of Fano-resonant metasurfaces using plasmonic response of graphene in the mid-infrared," *Nano Lett.*, vol. 13, no. 3, pp. 1111–1117, Mar. 2013.
[24] W. Gao, J. Shu, C. Qiu, and Q. Xu, "Excitation of plasmonic waves in graphene by guided-mode resonances," *ACS Nano*, vol. 6, no. 9, pp. 7806–7813, Sep. 2012.
[25] M.-S. Kwon and S.-Y. Shin, "Simple and fast numerical analysis of multilayer waveguide modes," *Opt. Commun.*, vol. 233, no. 1–3, pp. 119–126, Mar. 2004.